AD-A064 175 STANFORD UNIV CALIF INST FOR PLASMA RESEARCH F/G 20/4
SIMULATION OF THREE-DIMENSIONAL TURBULENT FLOWS WITH A VORTEX-I--ETC(U)
JAN 79 B COUET, O BUNEMAN, A LEONARD N00014-78-C-0272
UNCLASSIFIED SU-IPR-715 NL

| OF /
AD
A064175

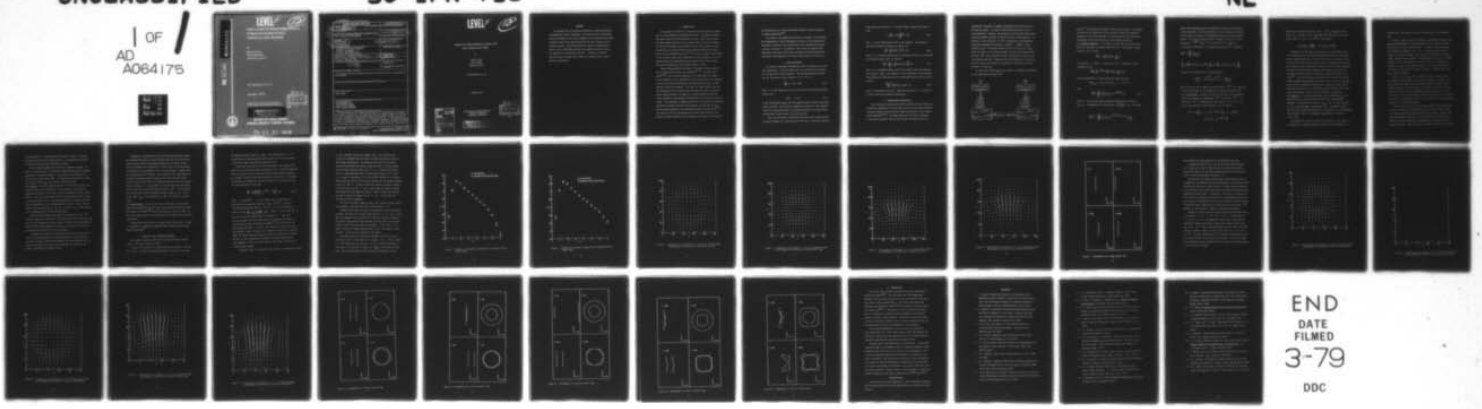

END
DATE
FILMED
3-79
DDC

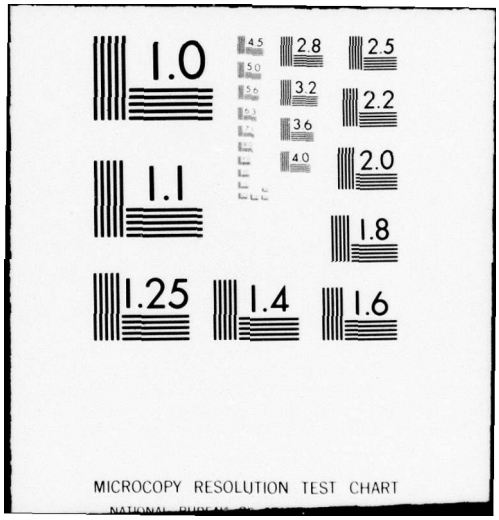
1.0
1.1
1.25
1.4
1.6
1.8
2.0
2.2
2.5
2.8
3.2
3.6
4.0
4.5
5.0
MICROCOPY RESOLUTION TEST CHART

LEVEL II

12

SIMULATION OF THREE-DIMENSIONAL TURBULENT FLOWS WITH A VORTEX-IN-CELL METHOD

by

Benoit Couët
Oscar Buneman
Anthony Leonard

SU-IPR Report No. 715

January 1979

INSTITUTE FOR PLASMA RESEARCH
STANFORD UNIVERSITY, STANFORD, CALIFORNIA

UNCLASSIFIED

SECURITY CLASSIFICATION OF THIS PAGE (When Data Entered)

REPORT DOCUMENTATION PAGE

READ INSTRUCTIONS BEFORE COMPLETING FORM

(14) REPORT NUMBER: SU-IPR ~~Report No.~~ 715

2. GOVT ACCESSION NO.

3. RECIPIENT'S CATALOG NUMBER

(6) 4. TITLE (and Subtitle)

SIMULATION OF THREE-DIMENSIONAL TURBULENT FLOWS WITH A VORTEX-IN-CELL METHOD.

5. TYPE OF REPORT & PERIOD COVERED: Scientific (9) Technical rept.,

6. PERFORMING ORG. REPORT NUMBER

(10) 7. AUTHOR(s)

Benoit/Couet,
Oscar/Buneman
Anthony/Leonard

(15) 8. CONTRACT OR GRANT NUMBER(s): N0014-78-C-0272 new

9. PERFORMING ORGANIZATION NAME AND ADDRESS

Institute for Plasma Research,
Stanford University, CA,
Stanford, California 94305

10. PROGRAM ELEMENT, PROJECT, TASK AREA & WORK UNIT NUMBERS

11. CONTROLLING OFFICE NAME AND ADDRESS

Mathematical & Information Sciences Div.
Office of Naval Research, 800 N. Quincy St.,
Arlington, Virginia 22217

(11) 12. REPORT DATE: January 1979

13. NUMBER OF PAGES: 35

14. MONITORING AGENCY NAME & ADDRESS (if different from Controlling Office)

(12) 38p.

15. SECURITY CLASS. (of this report): Unclassified

15a. DECLASSIFICATION/DOWNGRADING SCHEDULE

16. DISTRIBUTION STATEMENT (of this Report)

This document has been approved for public release and sale; its distribution is unlimited.

17. DISTRIBUTION STATEMENT (of the abstract entered in Block 20, if different from Report)

18. SUPPLEMENTARY NOTES

TECH; OTHER

19. KEY WORDS (Continue on reverse side if necessary and identify by block number)

THREE-DIMENSIONAL
INCOMPRESSIBLE FLOW
VORTEX-IN-CELL METHOD
FAST FOURIER TRANSFORM

20. ABSTRACT (Continue on reverse side if necessary and identify by block number)

A new method for the numerical simulation of three-dimensional incompressible flows is described. Our vortex-in-cell (VIC) method traces the motion of the vortex filaments in the velocity field these filaments create on an Eulerian mesh via the fast integration of a Poisson equation. By incorporating the viscous or subgrid-scale effects into a filtering procedure, the computed scales of motion are assumed to be essentially inviscid. Results on tracing a periodic array of single vortex rings are compared with a Green's function calculation.

DD FORM 1 JAN 73 1473 EDITION OF 1 NOV 65 IS OBSOLETE

UNCLASSIFIED 332 630

SECURITY CLASSIFICATION OF THIS PAGE (When Data Entered)

AB

LEVEL II

12

SIMULATION OF THREE-DIMENSIONAL TURBULENT FLOWS WITH A VORTEX-IN-CELL METHOD

by

Benoit Couët
Oscar Buneman
Anthony Leonard

SU-IPR Report No. 715

January 1979

Institute for Plasma Research
Stanford University
Stanford, California

ABSTRACT

A new method for the numerical simulation of three-dimensional incompressible flows is described. Our vortex-in-cell (VIC) method traces the motion of the vortex filaments in the velocity field these filaments create on an Eulerian mesh via the fast integration of a Poisson equation. By incorporating the viscous or subgrid-scale effects into a filtering procedure, the computed scales of motion are assumed to be essentially inviscid. Results on tracing a periodic array of single vortex rings are compared with a Green's function calculation.

1. INTRODUCTION

In this paper, we describe a new method for the numerical simulation of three-dimensional incompressible flows. Our approach differs from other numerical fluid simulations in that, rather than solving the Navier-Stokes equations on an Eulerian mesh, we trace the motion of the vortex filaments in the velocity field these filaments create. In addition, the velocity field is not calculated directly by Biot-Savart's law of interaction as in[1,2,3], but by creating a mesh-record of the vorticity field, then integrating a Poisson equation to get the stream function and generating a mesh-record of the velocity field. The vortex filaments are then stepped forward in time.

Vortex pushing methods--as distinct from Navier-Stokes methods--have a history of success in two dimensions[4-8]. In three dimensions[1,2,3], one of us has applied it to a small number of simple vortex filaments, but at considerable cost because of the time required to sum all the mutual Biot-Savart type interactions between the many elements in all the filaments. The "cell" or "mesh" method speeds up the calculation of the interactions and allows the three dimensional vortex pushing method to be applied to a space densely filled with vortex filaments, each filament being resolved in fine detail along its length. The techniques of making optimal use of the mesh for evaluating interactions between different fluid elements are the same as those used by plasma physicists for calculating particle interactions[9-12]. In creating a code for the evaluation of local flow fields due to a family of vortex filaments we have therefore taken over the principles

and architecture of a code developed for magnetic field evaluations in plasma simulations[12].

An outline of the remaining sections of the paper is as follows. The fundamentals of vorticity dynamics relevant to our technique are discussed in Section 2 and a description of the computational method is given in Section 3. In Section 4, the results of computational experiments involving vortex rings are presented and discussed while conclusions and suggestions for further work are given in Section 5.

2. BASIC PRINCIPLES

We assume an unbounded incompressible flow, fully periodic in the three dimensions. In each periodic box, the vorticity field consists of a collection of vortex filaments. The governing dynamic equation for the vorticity in these filaments, $\vec{\omega} = \nabla \times \vec{u}$, is

$$\frac{D\vec{\omega}}{Dt} = \vec{\omega} \cdot \nabla\vec{u} + \nu\nabla^2\vec{\omega} \qquad (2.1)$$

where ν is the viscosity and the velocity field is determined kinematically from

$$\nabla^2\vec{u} = - \nabla \times \vec{\omega} \qquad (2.2)$$

In the following we assume that the computed scales of motion are essentially inviscid. Any viscous or subgrid-scale effects on the computed fields are incorporated into the filtering procedure introduced below and described in more detail in the next section.

Thus, from the Kelvin and Helmholtz theorems, each filament may be followed throughout the time history of the flow in a material reference

frame with the circulation Γ of each filament remaining constant in time.

$$\Gamma = \oint \vec{u} \cdot d\vec{\ell} = \iint_A \vec{\omega} \cdot d\vec{A} \tag{2.3}$$

Here A is the cross-section area of the filament. In particular, the vorticity field in each box is taken to be

$$\vec{\omega}(\vec{r}) = \int G(\vec{r}-\vec{r}') \, \tilde{\vec{\omega}}(\vec{r}') \, d\vec{r}' \tag{2.4}$$

where G is a filter function and the unfiltered vorticity is generated by the space curves $\vec{r}_i(\xi)$ as follows:

$$\tilde{\vec{\omega}}(\vec{r}) = \sum_i \Gamma_i \oint \delta(\vec{r}-\vec{r}_i(\xi)) \frac{\partial \vec{r}_i}{\partial \xi} \, d\xi \, . \tag{2.5}$$

Here ξ is a parameter which traces each filament along its length at any instant in time. The summation is over individual vortex filaments. The evolution of each space curve is determined from the filtered velocity by

$$\frac{\partial \vec{r}_i(\xi)}{\partial t} = \int G(\vec{r}_i-\vec{r}') \, \vec{u}(\vec{r}') \, d\vec{r}' \tag{2.6}$$

with $\vec{u}$ determined from (2.2). Using the same filter G in (2.6) as in (2.4) will ensure momentum conservation.

3. COMPUTATIONAL DESCRIPTION

For a variety of reasons, the vorticity field and other fields are conveniently expressed in Fourier space, just as in the more successful numerical attacks on the turbulence problem by solution of the Navier-Stokes equation[13-17]. The main reason why the velocity component is recorded in spectral form is that calculus (differentiation and

integration) translates to algebra (multiplication and division) in the spectral domain. Of course, this implies periodicity in all three dimensions. However, the potential of getting away from finite-difference methods by means of spectra cannot be fully realized. In principle, local evaluation of $F(\vec{r})$ by summation of individually calculated trigonometric functions $\sin(\vec{k}\cdot\vec{r})$, $\cos(\vec{k}\cdot\vec{r})$ would eliminate grids. In practice, when this has to be done at a large number of places, as in vortex tracing, one must first transform the spectrum $F(\vec{k})$ onto some grid and then interpolate for arbitrary $\vec{r}$ from nearest grid data. Likewise, when the excitation of a spectrum by local sources of vorticity is evaluated, a similar act of interpolation is called for.

At this point, before going into details, a schematic description of the computation is given below.

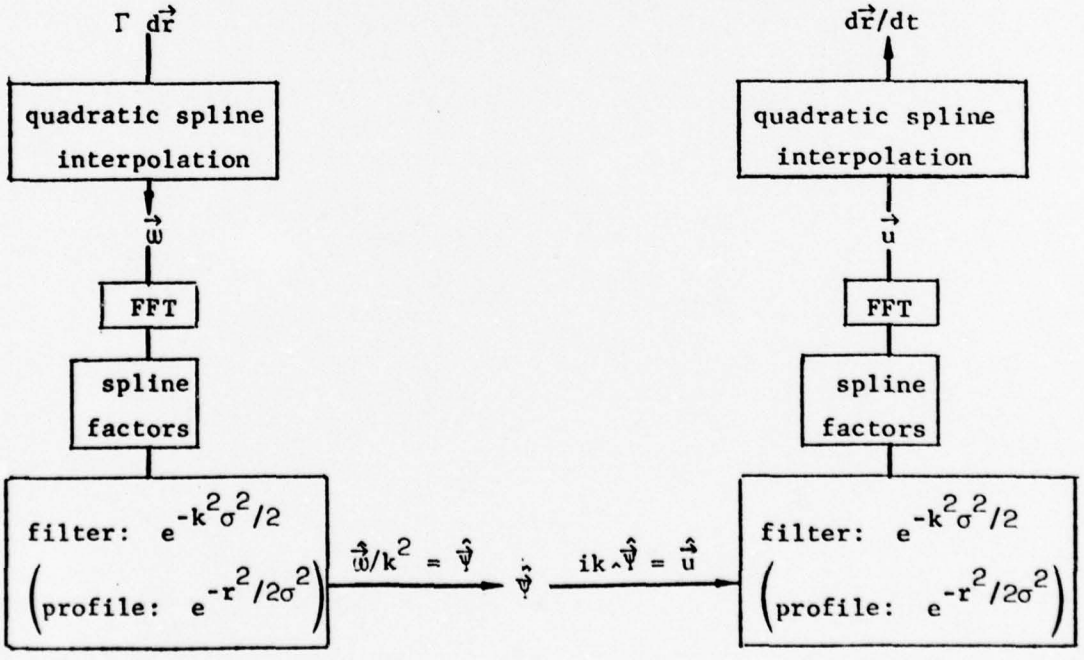

where $\hat{\vec{\Psi}}$ is the Fourier transform of the vector potential. The different parts of the scheme will now be explained, namely the numerical modeling of the vortex filaments, the interpolations that take place, the shaping of the vortices and the time-stepping procedure.

3.1 Filament Modeling: In our model, one describes each vortex filament by a succession of closely spaced markers. Considering a single vortex in (2.5), we have

$$\tilde{\vec{\omega}}(\vec{r}) = \Gamma \oint \delta(\vec{r}-\vec{r}(\xi)) \frac{\partial \vec{r}}{\partial \xi} \, d\xi$$

at an instant t, where Γ is given by (2.3). Taking the Fourier transform, we get

$$\tilde{\vec{\omega}}(\vec{k}) = \int e^{-i\vec{k}\cdot\vec{r}} \, \Gamma \oint \delta(\vec{r}-\vec{r}(\xi)) \frac{\partial \vec{r}}{\partial \xi} \, d\xi \, d\vec{r}$$

If we now discretize $\vec{r}$ into piece-wise linear sections,

$$\vec{r}(\xi)_{j,j-1} = \xi \, \vec{r}_j + (1-\xi) \, \vec{r}_{j-1} \quad , \quad 0 \le \xi \le 1 \, ,$$

then

$$\tilde{\vec{\omega}}(\vec{k}) = \sum_{j=1}^{m} \Gamma \int_0^1 (\vec{r}_j - \vec{r}_{j-1}) \, e^{-i\vec{k}\cdot\vec{r}(\xi)} \, d\xi \qquad (3.1)$$

where m is the total number of markers describing the filament; $\vec{r}_m = \vec{r}_o$. Integrating (3.1) and letting $\vec{k}\cdot\frac{(\vec{r}_j-\vec{r}_{j-1})}{2} = \epsilon_j$, we obtain:

$$\tilde{\vec{\omega}}(\vec{k}) = \Gamma \sum_{j=1}^{m} (\vec{r}_j - \vec{r}_{j-1}) \, e^{-i\vec{k}\cdot(\vec{r}_j+\vec{r}_{j-1})/2} \, \frac{\sin \epsilon_j}{\epsilon_j} \, .$$

Rather than interpolating each trigonometric function in the Fourier series separately, it is more efficient to first distribute vorticity onto the grid according to an interpolation process and then perform an FFT. To do this, we must be able to express $\sin \epsilon_j/\epsilon_j$ as combination of $e^{-i\vec{k}\cdot\vec{f}}$ where $\vec{f}$ is a function of $\vec{r}_j$ and $\vec{r}_{j-1}$. In our case, evaluating (3.1) by gaussian quadrature[18], we obtain

$$\tilde{\vec{\omega}}(\vec{k}) = \Gamma \sum_{j=1}^{m} \frac{(\vec{r}_j - \vec{r}_{j-1})}{2}$$

$$\times \left\{ e^{-i\vec{k}\cdot\frac{1}{2}\left[(1+3^{-\frac{1}{2}})\vec{r}_j + (1-3^{-\frac{1}{2}})\vec{r}_{j-1}\right]} + e^{-i\vec{k}\cdot\frac{1}{2}\left[(1-3^{-\frac{1}{2}})\vec{r}_j + (1+3^{-\frac{1}{2}})\vec{r}_{j-1}\right]} \right\}$$

Indeed this is equivalent to the approximation,

$$\frac{\sin \epsilon_j}{\epsilon_j} \simeq \frac{e^{-i\epsilon_j 3^{-\frac{1}{2}}} + e^{i\epsilon_j 3^{-\frac{1}{2}}}}{2} = \cos\left(\frac{\epsilon_j}{3^{\frac{1}{2}}}\right)$$

What we want now is to replace the pure harmonic $e^{i\vec{k}\cdot\vec{r}}$ for arbitrary $\vec{r}$ by an approximant to be evaluated on the discrete spatial mesh.

3.2 Interpolation: In each of the three dimensions we use quadratic spline interpolation to approximate e^{ikx} in terms of e^{ikn}. In particular e^{ikx} is represented in the interval $n - \frac{1}{2} \le x \le n + \frac{1}{2}$ as the superposition of three parabolic arcs as follows:

$$e^{ikx} \simeq S(k)\left[\frac{1}{2}(x - n + \frac{1}{2})^2 e^{ik(n+1)} + \left(\frac{3}{4} - (x - n)^2\right)e^{ikn} + \frac{1}{2}(n + \frac{1}{2} - x)^2 e^{ik(n-1)}\right]$$

Rather than choosing the function $S(k)$ to force agreement at the point $x=n$, we select $S(k)$ to minimize the mean square error over the interval $n - \frac{1}{2} \leq x \leq n + \frac{1}{2}$[12]. This leads to:

$$S(k) = \left(\frac{2}{k} \sin \frac{k}{2}\right)^3 \Big/ \left(1 - \sin^2 \frac{k}{2} + \frac{2}{15} \sin^4 \frac{k}{2}\right)$$

Therefore, the three nearest grid points in each dimension (27 in all) will share the vorticity distribution according to the spline function weighting on them. In other words, this is a particular way to distribute a finite-sized vorticity on its neighboring grid points. The quadratic spline weighting is superior to the zero-order weighting (NGP model) and first-order weighting (CIC model) in the sense of creating less field-noise and resulting in smoother simulation functions[19]. This is an obvious conclusion since vorticity is now distributed among three grid points instead of one or two as in the other models and the interpolated distribution is quadratic rather than a piece-wise step function, or first-order linear function, with discontinuous derivatives. There is also a reduction of aliassing.

3.3 Shaping: It is intuitively obvious that low-$|\vec{k}|$ harmonics are interpolated by a certain tabulation mesh better than high-$|\vec{k}|$ harmonics. Aliassing sets a limit at $k_{max} = \pi/\Delta$ for each component of $\vec{k}$ ($\Delta \equiv$ mesh spacing): any harmonic with a k-component higher than this will be misinterpreted by the interpolator as a corresponding lower harmonic with all k-components lying within the interval $(-\pi/\Delta\ ,\ \pi/\Delta)$.

The effects of a finite cut-off of the spectrum on the physics to be computed is an important question separate from the question of

interpolation. Two aspects of the cut-off problem are worth emphasizing.

Firstly, a sharp cut-off in $\vec{k}$-space is undesirable (no matter how perfectly each harmonic is evaluated) because it surrounds the objects that interact via the field with halos in $\vec{r}$-space. The halos decay only weakly with distance, like $1/r$. If instead, the spectrum is brought to zero more smoothly, say at least parabolically, such halos become attenuated more strongly. A bell-shaped cut-off factor $\hat{G}^2(|\vec{k}|)$ suggests itself. Consequently, even if the object of interpolation studies is to push up the maximum usable k, it should concentrate on performance in the range of low and intermediate $|\vec{k}|$; $|\vec{k}|$-values near k_{max} become irrelevant.

Secondly, any cut-off factor $\hat{G}^2(|\vec{k}|)$ implies a shape for the interacting vortices which is the Fourier transform of $\hat{G}(|\vec{k}|)$: this is so because the shape enters the field interaction process twice, namely both when the field harmonics are excited by the local sources (vortices) and when the field harmonics react back on them. So, any such factor in the spectral domain (introduced primarily for the purpose of fitting the field harmonics into a finite computer) can be interpreted physically as vorticity-spreading.

There are good reasons for introducing shapes of the interacting elements even when no interpolation is used at all and spectral data are evaluated precisely, without grids and tabulations. Firstly, the interacting "fluid elements" in the real world are usually much more numerous than those that can be accommodated in a computer with its peripheral storage. Each element in the computer stands in for a swarm

of real elements. It should therefore be given a spread. Secondly, the binary interaction of "fluid elements" is unrealistically strong if they are treated as delta-functions in space.

We note that the shape factor should be isotropic in space: it knows no coordinate axes. We choose an approximately gaussian profile, equivalent to a gaussian shape in (x,y,z)-space, but brought to a strict zero at some maximum $|\vec{k}|$. De-emphasizing the harmonics close to, and just below k_{max} will further reduce aliassing.

3.4 Solving: If we now consider equation (2.2) in Fourier space, the velocity field at the location of a "vortex-marker" is obtained by weighting the entries in the table of spline amplitudes with the spline weights. The latter are deduced from the relative position of a vortex in its interpolation cell. The spline amplitudes are obtained from the velocity harmonics by first multiplying with a factor $S(k_x)$ and two similar factors which have k_y and k_z in place of k_x , then calling a three-dimensional FFT on the resulting array.

The same factors appear again when the displacement of the k^{th} vorticity harmonic is calculated. The interpolation can be done for the sum of all the harmonics, and the tables into which one interpolates are then the FFT's of the harmonics of vorticity, modified by the factors insuring best mean square fit in each dimension.

In going from the table of spline amplitudes for vorticity to the table of spline amplitudes for velocity harmonics, one therefore has not only to perform a forward and backward FFT, with equation (2.2) in $\vec{k}$-space in between, but one must also introduce the squares of the spline fitting factors indicated above.

Similarly, we mentioned that any vorticity shaping factor should be introduced both when the local velocity field action on the distributed vorticity cloud is evaluated and when its excitation of the vorticity harmonics is accumulated. In both cases, one could perform a convolution in (x,y,z)-space, but is is much quicker to replace this by a multiplication in $\vec{k}$-space. The transform of the shape factor is therefore introduced squared along with the above mentioned spline fitting factors in the course of solving the equations for the velocity field in $\vec{k}$-space. It is convenient to introduce the (squared) shape factor along with the inverse Poisson operator $1/k^2$. In our present 16^3 code there are only 64 possible different values of k^2 in the sphere $|\vec{k}| \leq k_{max}$, so any function of $|\vec{k}|$ can readily be pretabulated.

3.5 Time-Stepping: So far in the code, we have been using the well known leap-frog method with the first step generated by Euler's method. This method is unstable[20] but was used mainly to test our code. In fact, we already noticed the instability of this scheme in our two-ring experiments.

Nevertheless, used with an occasional forward Euler step, it seems to be possible to suppress the weak instability associated with leap-frog differencing[1].

4. RESULTS OF THE COMPUTER EXPERIMENTS

The computer used was a CDC 7600 located at NASA-Ames Research Center. The present mesh size is 16^3.

A first test was done on a single vortex ring of radius R about the z-axis. Its center is initially located at (8,8,8) in our mesh

and thereafter moves along the z-axis. The circulation is $\Gamma = 2$. In particular we investigated the initial speed of the vortex ring as a function of radius and position around the ring.

To check the accuracy of our mesh technique we also computed the speed of the vortex ring using a continuum or Green's function approach. Since the filter we use in the mesh method is approximately gaussian, we consider a single vortex ring of gaussian cross-section. Following the procedure as defined by (2.4-2.6), we obtain as its filtered velocity of translation in free space

$$\frac{\partial \vec{r}}{\partial t} = \frac{\Gamma}{4\pi} \oint \frac{f(a)}{|\vec{r}-\vec{r}\,'|^3} (\vec{r}-\vec{r}\,') \times \frac{\partial \vec{r}\,'}{\partial \xi} \, d\xi \qquad (4.1)$$

where $a = |\vec{r}-\vec{r}\,'|/2^{\frac{1}{2}}\sigma$, σ is the radius of the cross-section or the width of the gaussian filter and $f(a) = 2\pi^{-\frac{1}{2}} a e^{-a^2} - \mathrm{erf}(a)$. (It should be mentioned that for $\sigma^2 \ll R^2$, (4.1) can be approximated to yield $\frac{\partial \vec{r}}{\partial t} \approx \frac{\Gamma}{4\pi R}\left[\ln\left(\frac{8R}{\sigma}\right) - C\right]\vec{e}_z$ where $C = 1.058$ and $\vec{e}_z$ is the unit vector in the direction of translation z. Note that the actual speed of a thin vortex ring with a gaussian distribution of vorticity has been calculated by Saffman[21] and is given by the above formula but with $C = 0.558$. The difference is due to the fact that Saffman's result is based on the collective motion of an infinite number of vortex tubes with internal interaction between the filaments whereas our result represents the speed of a single computational ring filament). To (4.1), we then add the Biot-Savart contributions of the periodic images.

In Figures 1 and 2, we plot the total velocity of translation versus

R for a periodic array of our single rings. Our vortex-in-cell results are compared with the Green's function method given by (4.1) plus image contributions. The gaussian width used in the Green's function calculations was chosen to give the best fit to the vortex-in-cell results and was found to be $\sigma^2 = 1.1$ times the cell area. This is in good agreement with a theoretical estimate of $\sigma^2 = 12/\pi^2 \simeq 1.2$ based on a gaussian fit to the low $|\vec{k}|$ behavior of our filter. Recall that our filter is not strictly gaussian but is brought smoothly to zero at $|\vec{k}| = \pi$. Figure 1 shows the velocity recorded at points of the ring close to the x- and y-axes, where the velocity should be minimum since the images are closer. Figure 2 shows the velocity recorded at points 45 degrees off the x- and y-axes, where the velocity should be a maximum.

The four next figures show pictures of the initial velocity field in the middle of the mesh cells for a ring of radius $R = 4$.

Figures 3 and 4 show the field in the planes 1.5 mesh units below and above the plane of the ring, respectively at $z = 6.5$ and $z = 9.5$, where the magnitude of the field is the same but pointing in opposite directions, respectively toward and away from the center of the ring. Figures 5 and 6 show the field in the planes $x = 6.5$ and $x = 9.5$. Figure 7 shows the lateral vortex profile in the (x-z)-plane at four instants. We can see the constancy of the motion.

From these results, we derived an estimate of the CPU time per time step to move a vortex made of m markers. For $m = 360$, it takes 0.41 CPU seconds per time step; for $m = 720$, 0.48 CPU seconds per time step. So in general, it takes $0.34 + \frac{m}{5000}$ CPU seconds per time step. All calculations were done with leap-frog stepping in time

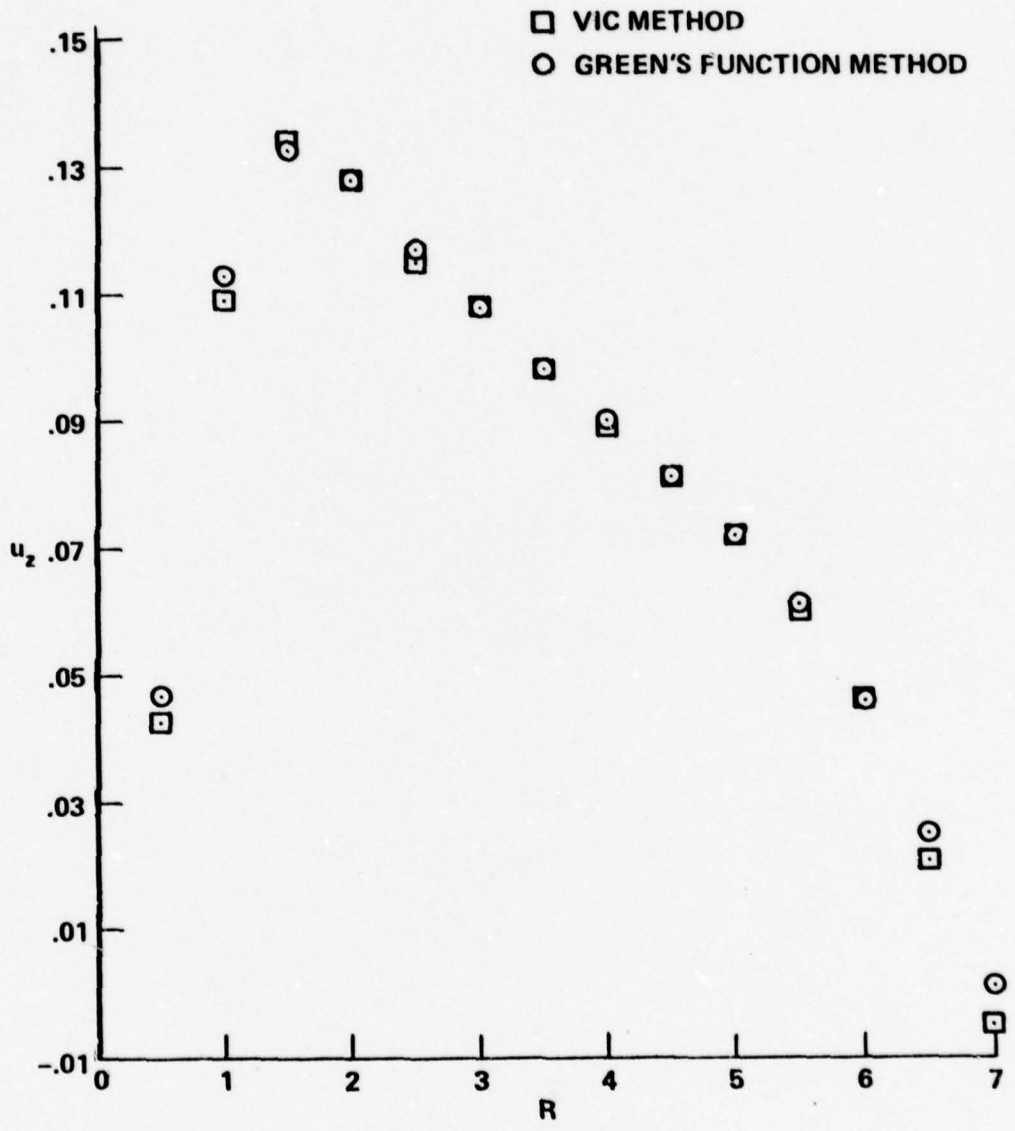

Figure 1. Velocity of translation (minimum) for a periodic array of single rings.

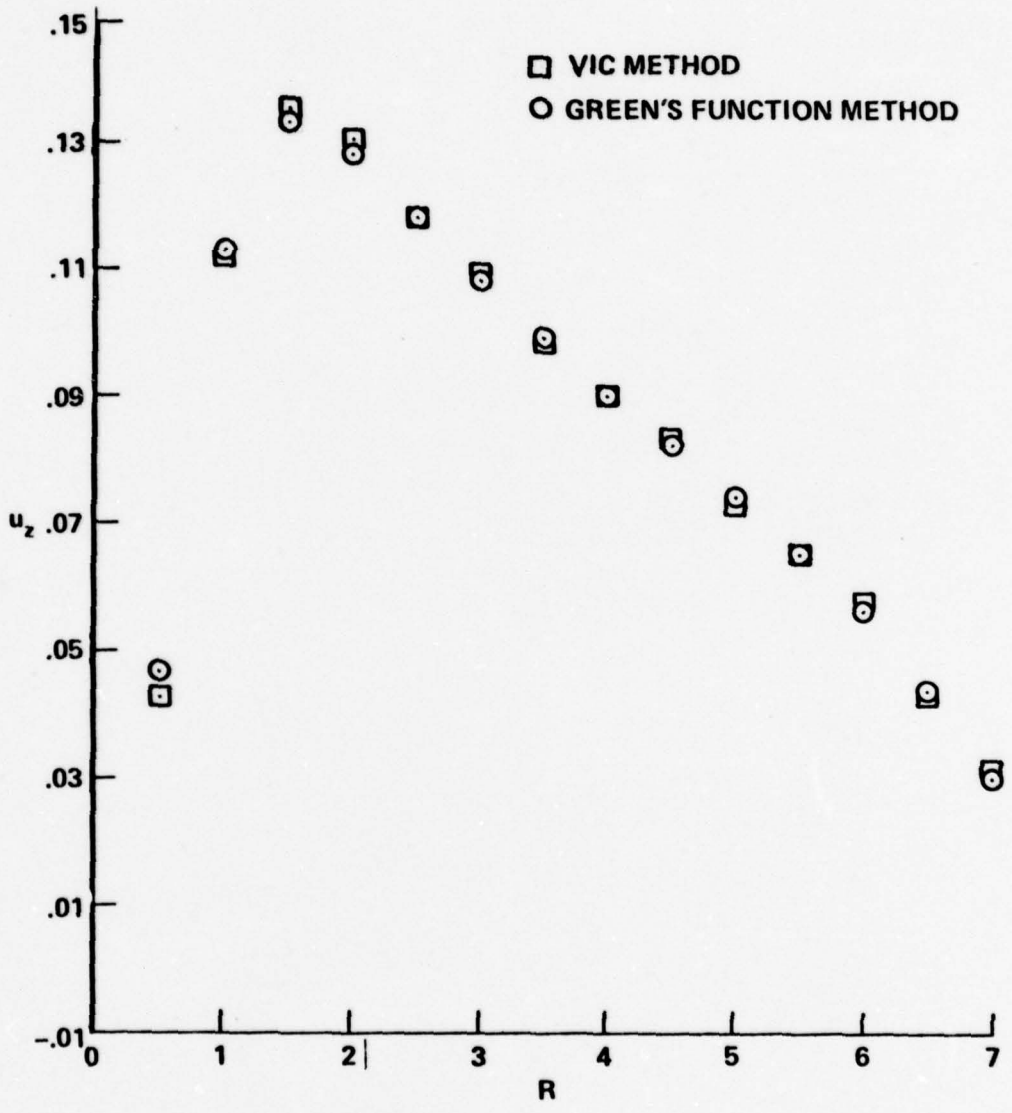

Figure 2. Velocity of translation (maximum) for a periodic array of single rings.

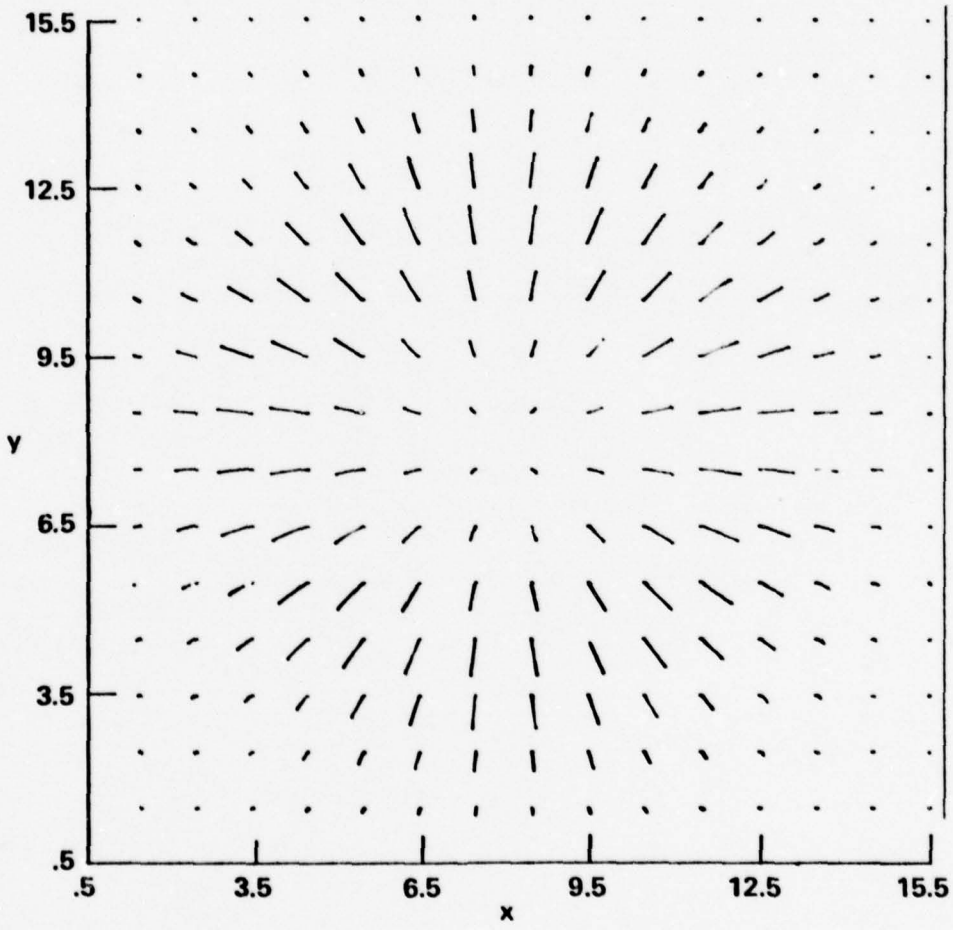

Figure 3. Projection on (x-y)-plane (z = 6.5) of the velocity field in the middle of the cells for a single vortex ring.

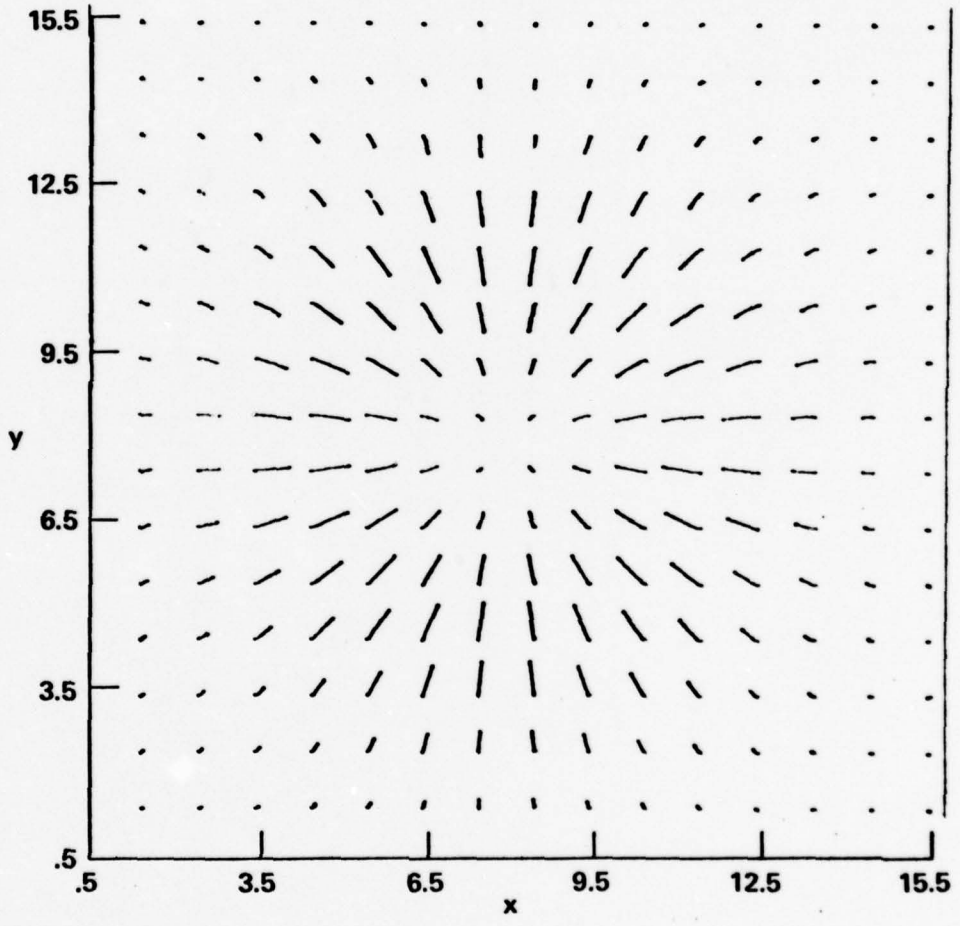

Figure 4. Projection on (x-y)-plane (z = 9.5) of the velocity field in the middle of the cells for a single vortex ring.

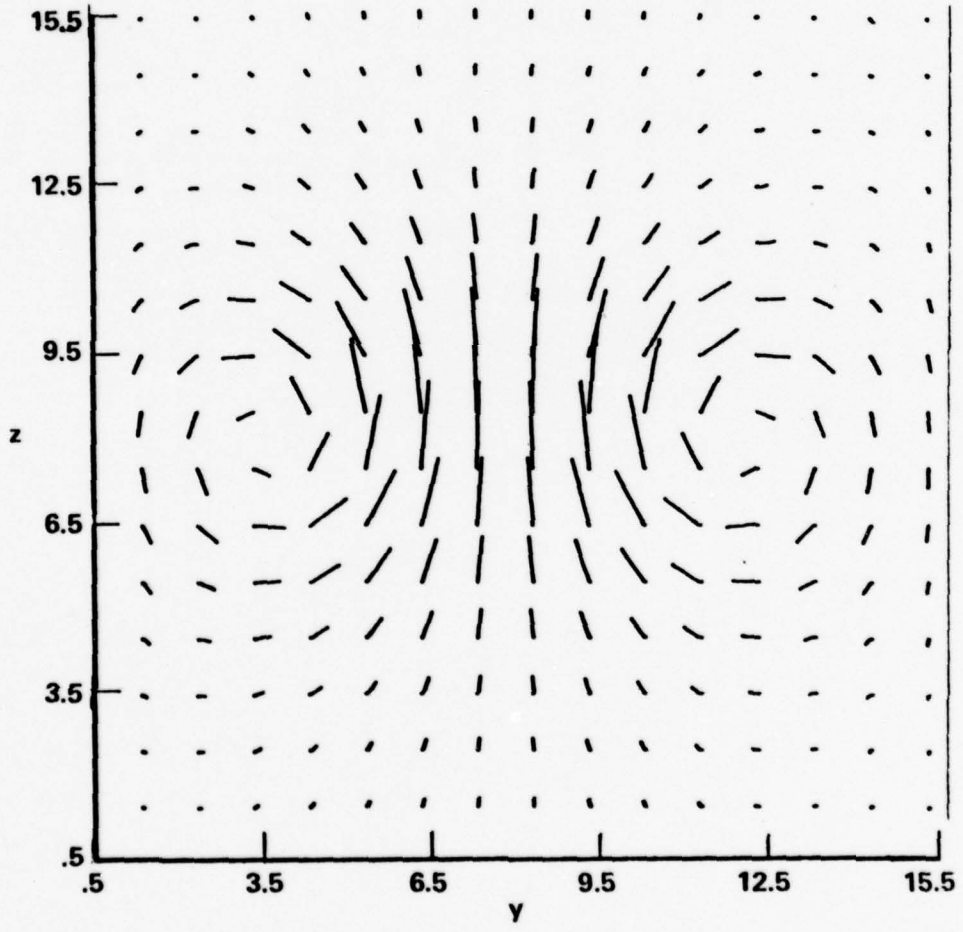

Figure 5. Projection on (y-z)-plane (x = 6.5) of the velocity field in the middle of the cells for a single vortex ring.

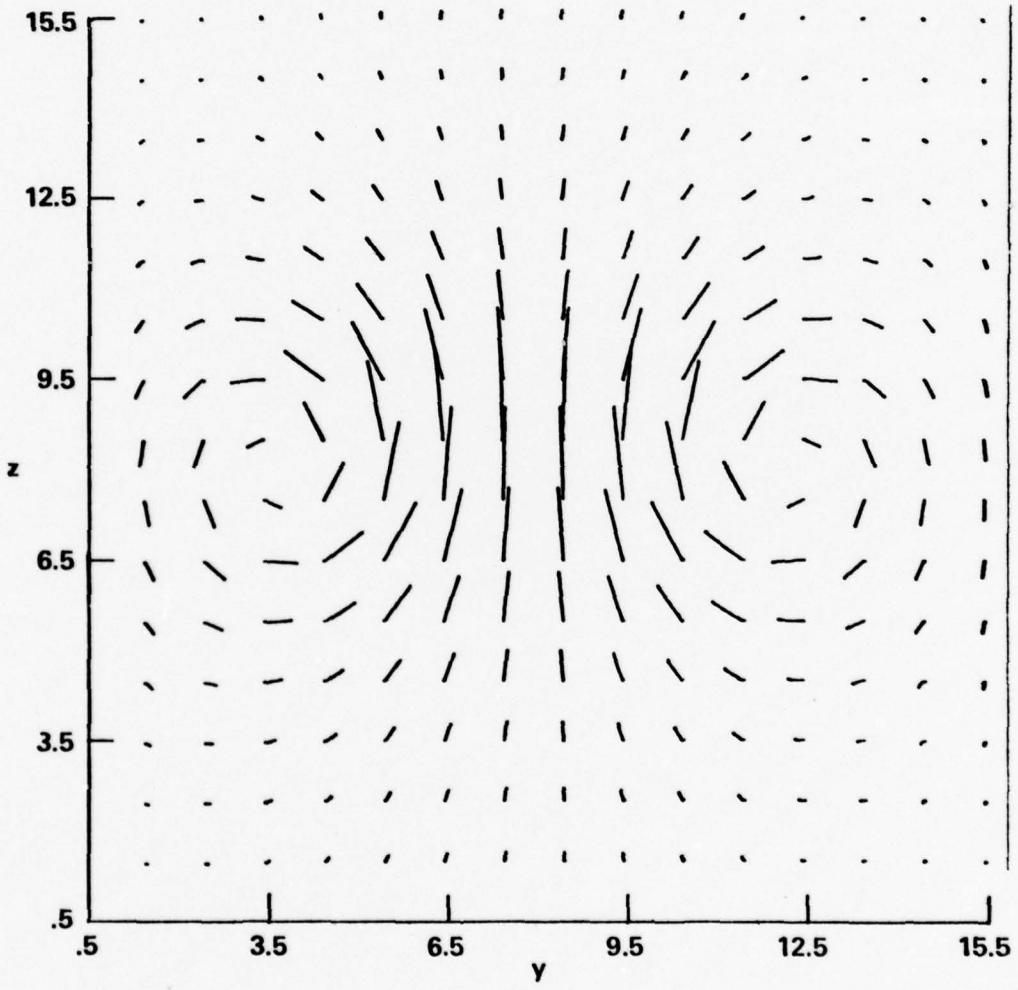

Figure 6. Projection on (y-z)-plane (x = 9.5) of the velocity field in the middle of the cells for a single vortex ring.

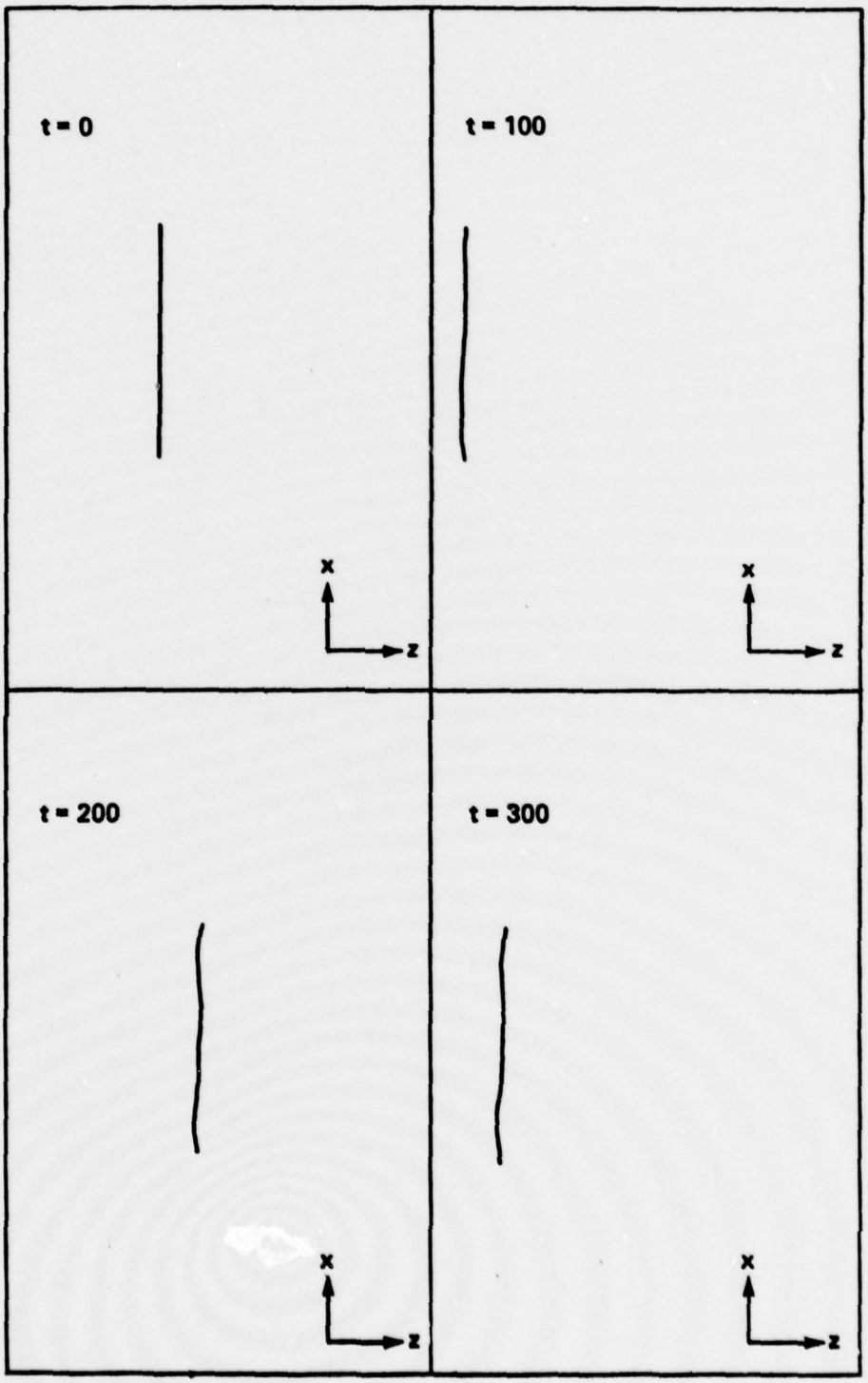

Figure 7. Displacement of a single vortex ring.

that involves only one evaluation of the derivative per step.

A second test was done on a set of two vortex rings of radius $R = 4$ about the z-axis. Their centers are initially located at (8,8,7) and (8,8,10) in the mesh and thereafter move also along the z-axis. Both have the same circulation $\Gamma = 2$.

We know that two similar vortex rings at some distance apart on a common axis of symmetry play the following game. The velocity field associated with the rear vortex ring has a radially outward component at the position of the front ring and so the radius of the front ring gradually increases (with Γ constant). This leads to a decrease in its velocity of translation, and there is a corresponding increase in the velocity of translation of the rear vortex which ultimately passes through the larger vortex and in turn becomes the front vortex. The maneuver is then repeated. Indeed, we observed that maneuver.

Figures 8, 9 and 10 show the initial velocity field respectively in the planes $z = 5.5$, $z = 8.5$ and $z = 11.5$. As expected, at $z = 5.5$ and $z = 11.5$, the magnitude of the field is the same but pointing in opposite directions, respectively toward and away from the center. At $z = 8.5$, centrally between the two rings, the field reaches a minimum. Figures 11 and 12 were taken at $x = 6.5$ and $x = 9.5$. The last five figures (13-17) show the displacement in the (x-z)-plane and the (x-y)-plane at ten instants. We see the rings going through each other repeatedly and the buildup of distortions due to the influence of images.

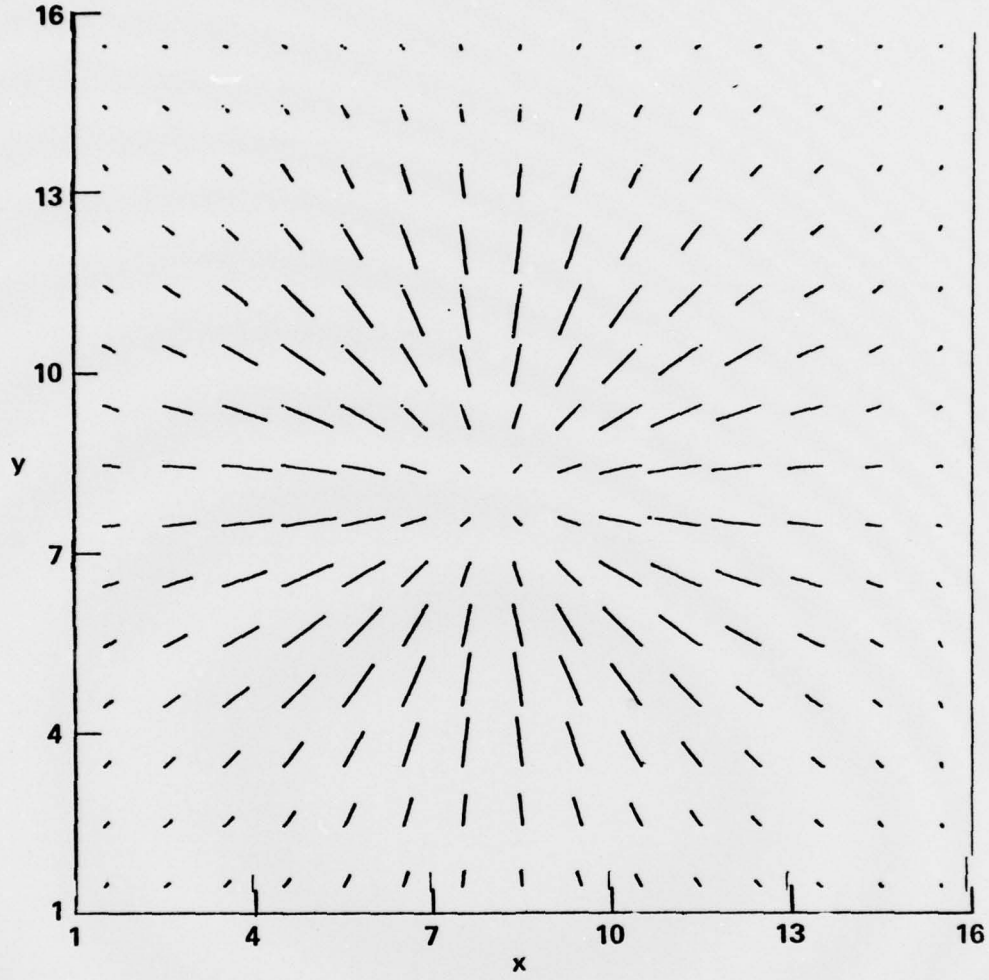

Figure 8. Projection on (x-y)-plane (z = 5.5) of the velocity field in the middle of the cells for a pair of vortex rings.

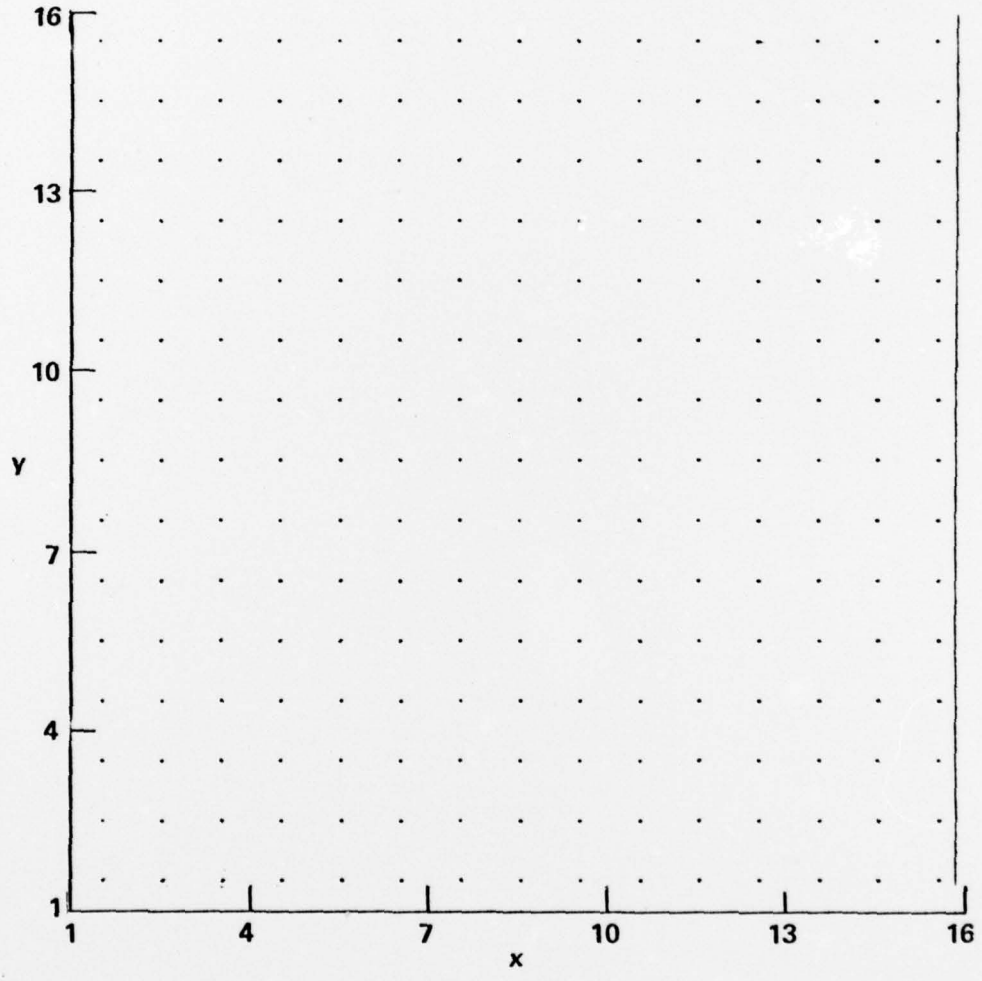

Figure 9. Projection on (x-y)-plane (z = 8.5) of the velocity field in the middle of the cells for a pair of vortex rings.

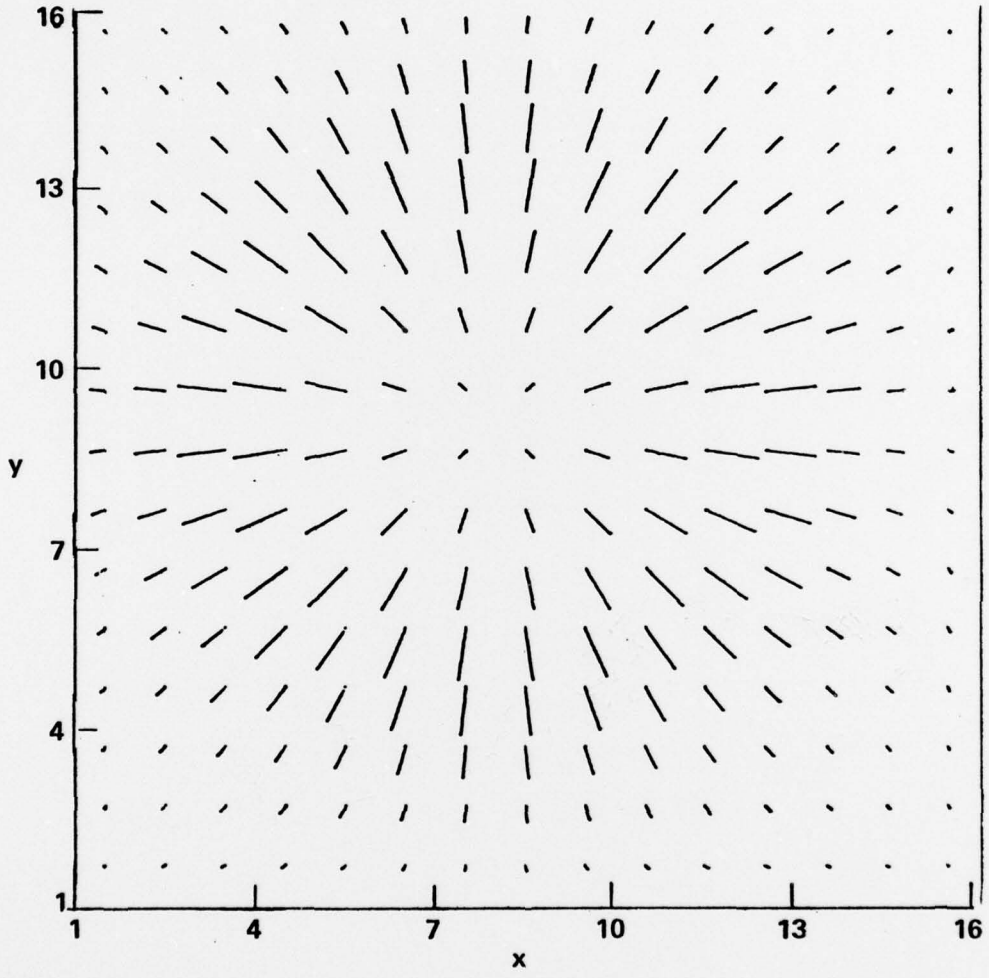

Figure 10. Projection on (x-y)-plane (z = 11.5) of the velocity field in the middle of the cells for a pair of vortex rings.

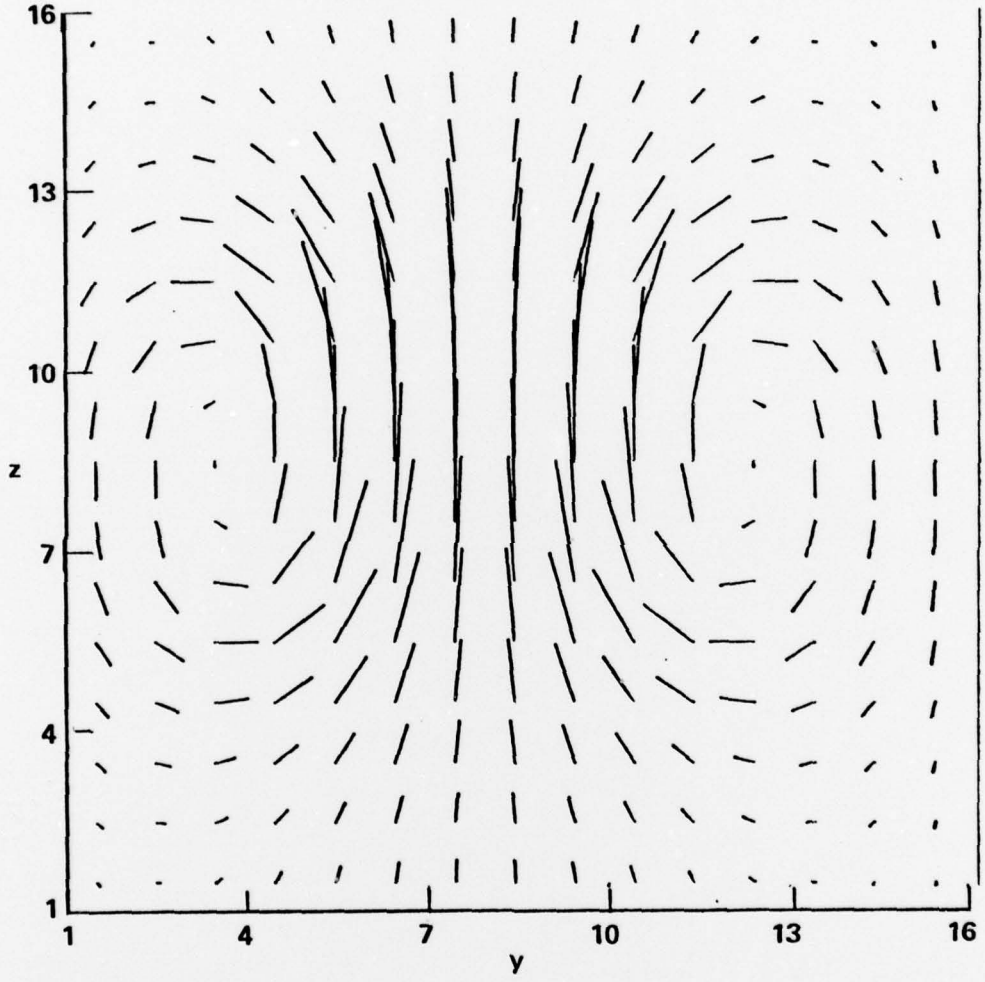

Figure 11. Projection on (y-z)-plane (x = 6.5) of the velocity field in the middle of the cells for a pair of vortex rings.

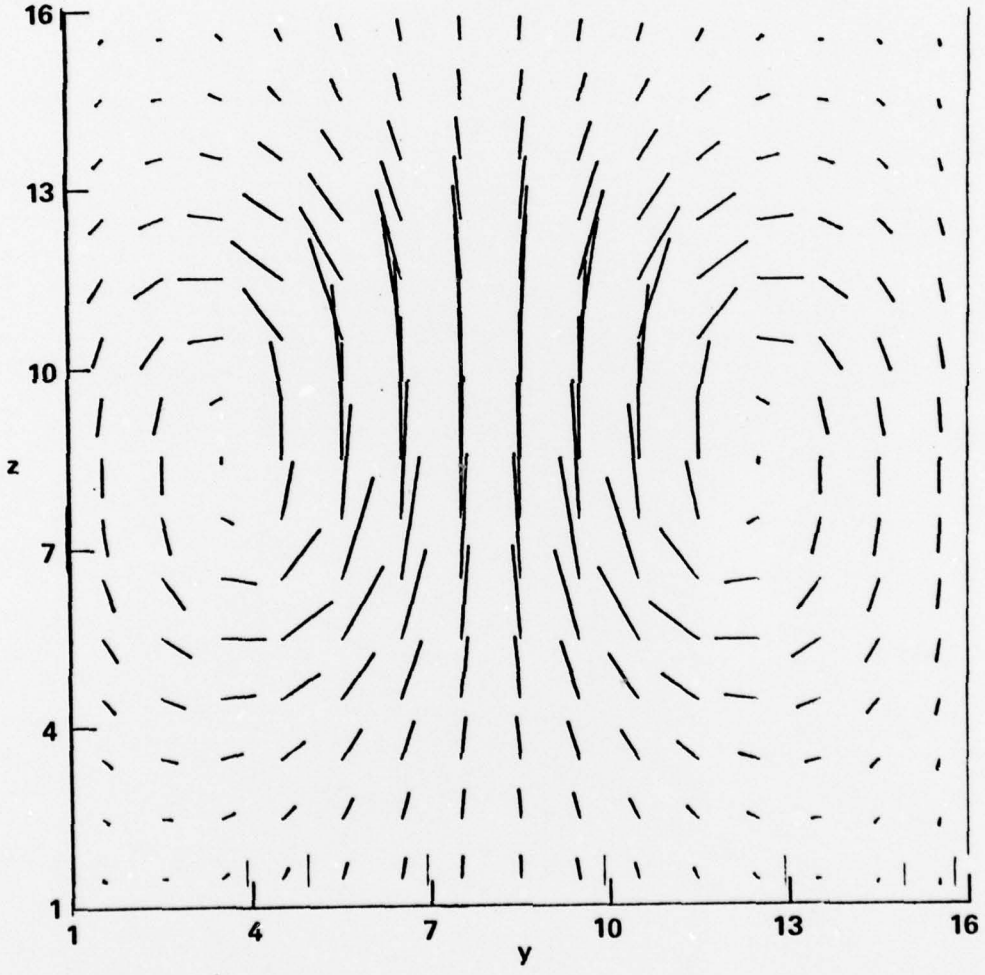

Figure 12. Projection on (y-z)-plane (x = 9.5) of the velocity field in the middle of the cells for a pair of vortex rings.

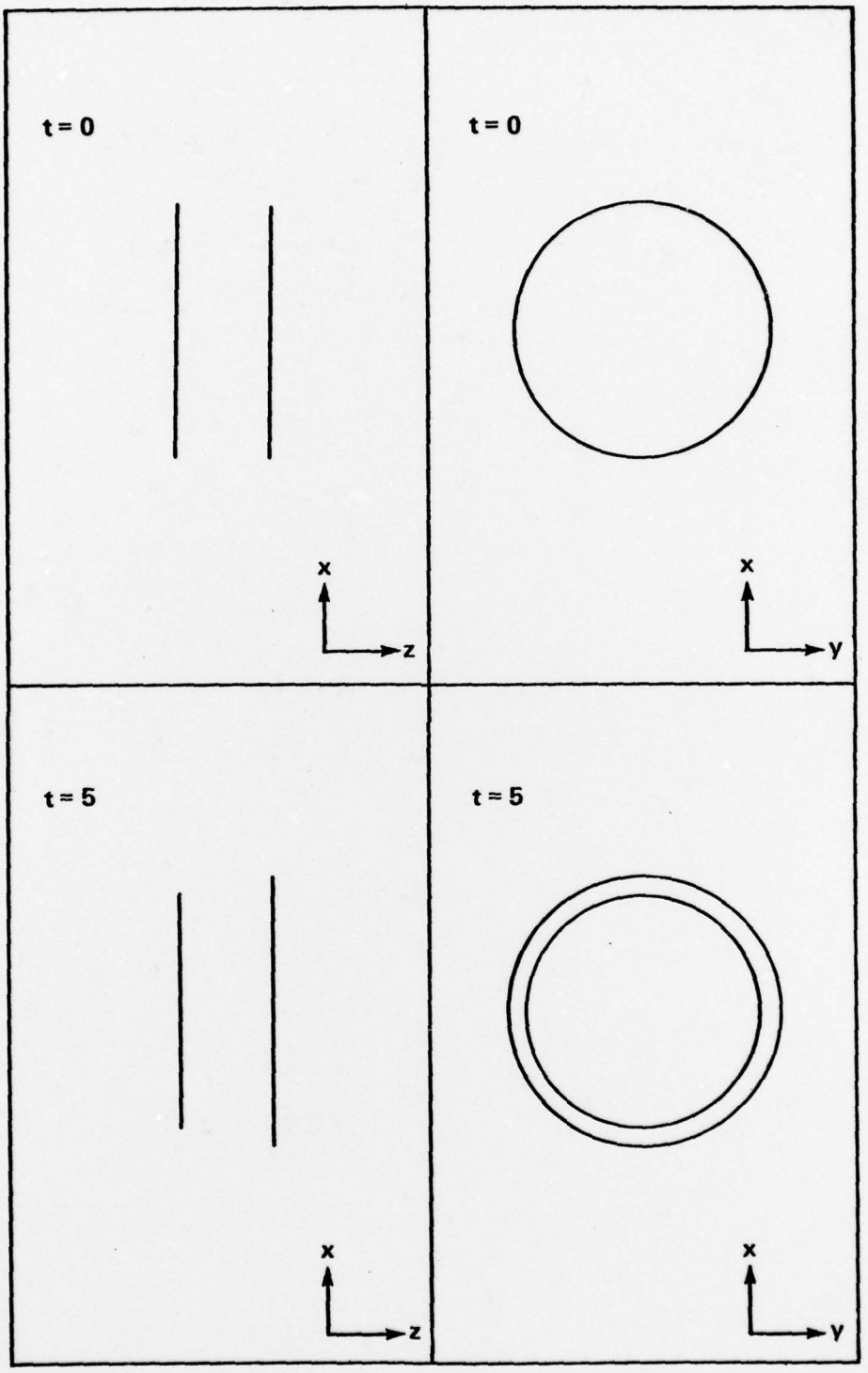

Figure 13. Displacement of a pair of vortex rings.

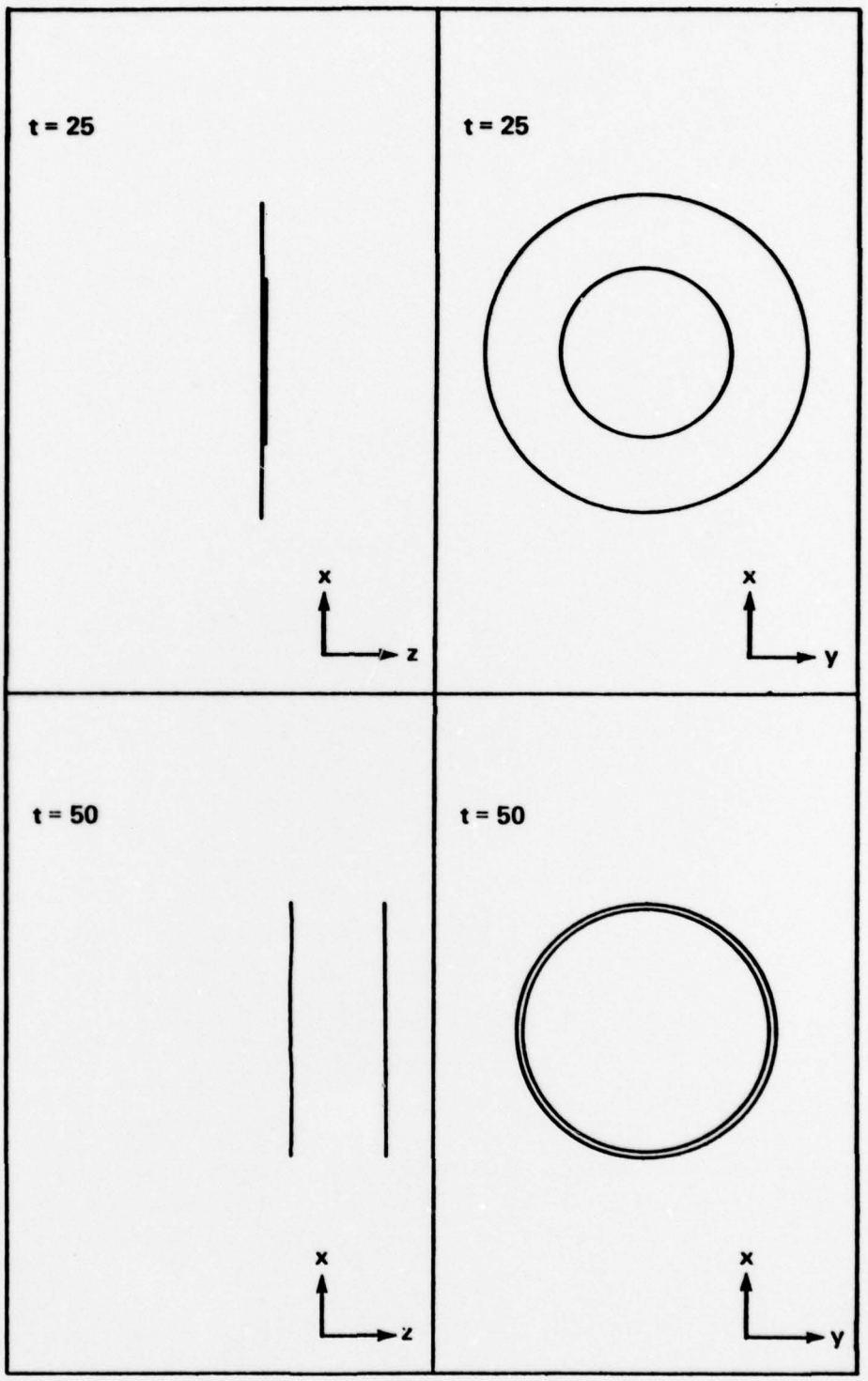

Figure 14. Displacement of a pair of vortex rings.

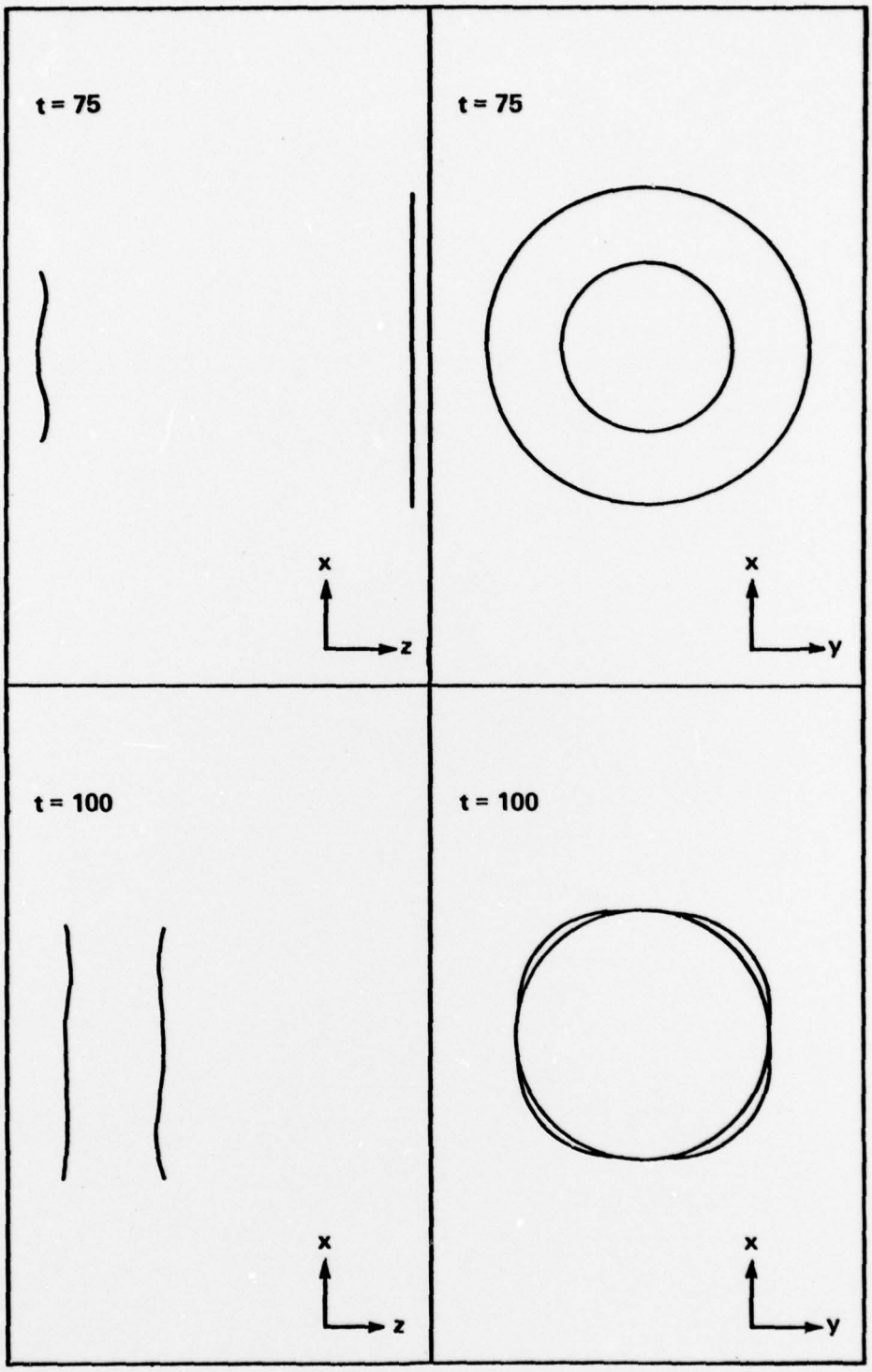

Figure 15. Displacement of a pair of vortex rings.

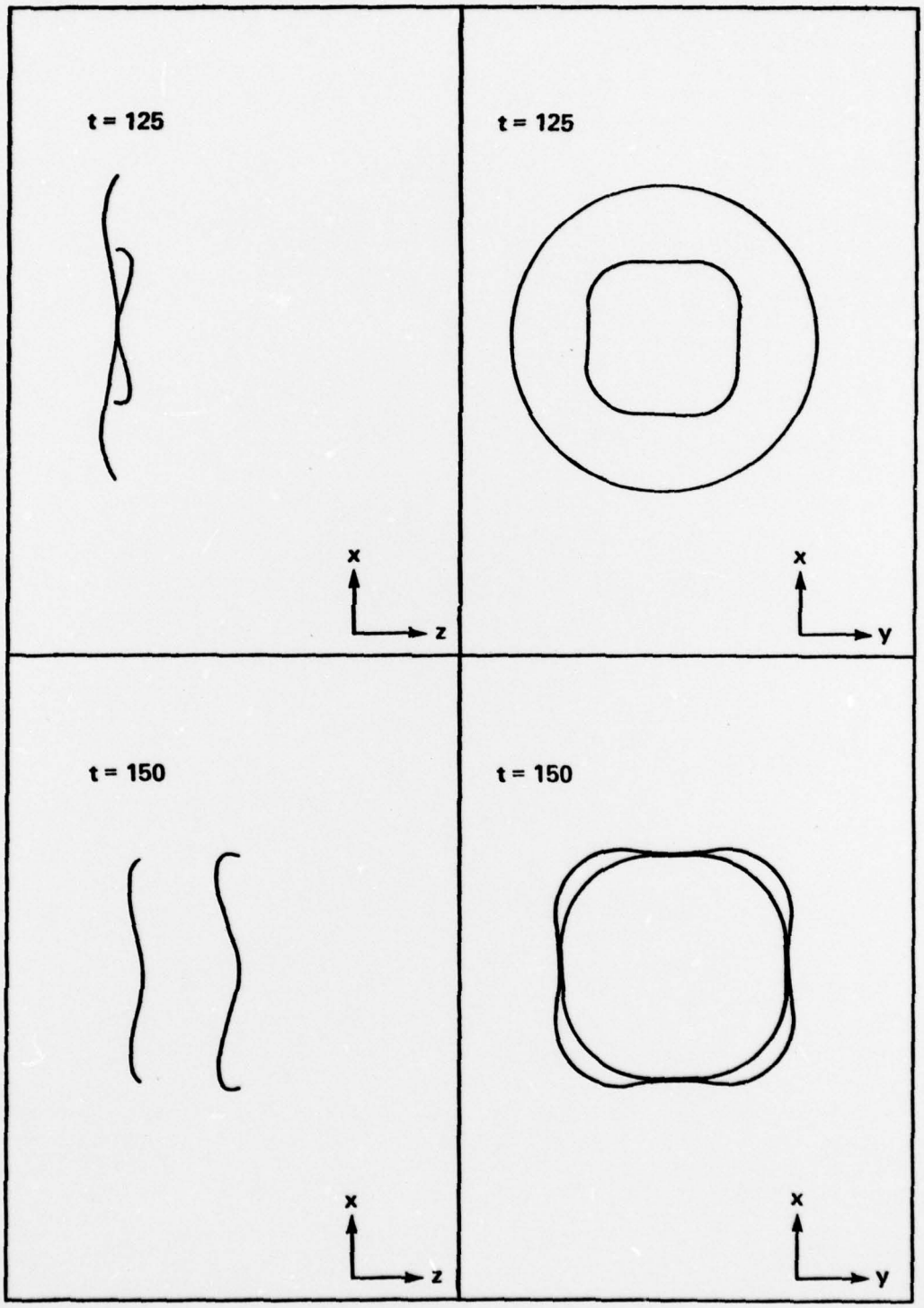

Figure 16. Displacement of a pair of vortex rings.

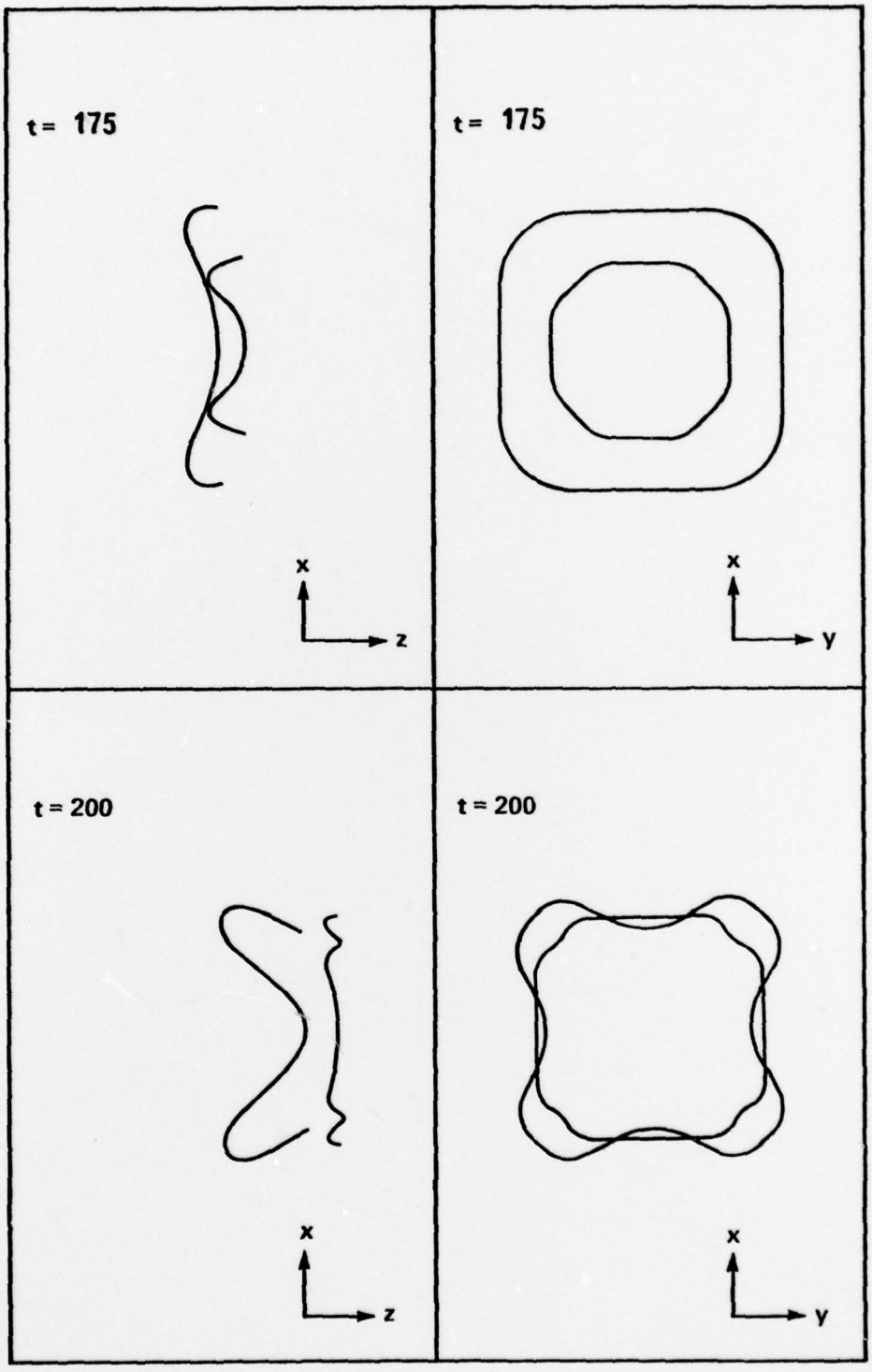

Figure 17. Displacement of a pair of vortex rings.

5. FURTHER WORK

As our next step, we shall initialize our code to the Taylor-Green vortex system[22]. This system has the three-dimensional periodic structure which is built into our first version of the code (by virtue of using complex FFT's). The Taylor-Green system has undergone both analytical study[13,23] and numerical study by methods other than ours[24,25]. The system is one of continuous vorticity, and it is important to represent such a continuum by a sufficient number of discrete vortex filaments. Sensitivity to the coarseness of this discretization (which is distinct from the discretization of the spatial mesh, and the time stepping) is to be explored.

One essential improvement of our code will be to proceed to finer meshes than 16^3. With a finer mesh one could then explore the evolution of vortex structures which have not been studied hitherto, and make reliable predictions from the computer output.

Several further code modifications are called for. The periodic boundaries ought to be changed so that one simulates (possibly vortex-shedding) planar walls in one or two of the three dimensions. This is done by replacing complex FFT's with readily available sine and cosine transforms. One would retain periodicity in the third dimension, having in mind the simulation of channel flow or flow through a re-entrant wind-tunnel of rectangular cross-section (but with curvature effects absent). Another variant is the simulation of "infinite" boundary conditions using similar approaches as in[26] and in[27].

ACKNOWLEDGEMENT

This work was initially supported by a NASA Interchange agreement with the Ames Research Center and subsequently by the Office of Naval Research.

REFERENCES

1. A. Leonard, "Numerical Simulation of Interacting, Three-Dimensional Vortex Filaments", Lecture Notes in Physics 35, Proc. 4th International Conference on Numerical Methods in Fluid Dynamics, 245-250, Springer-Verlag, Berlin (1975).
2. A. Leonard, "Simulation of Three-Dimensional Separated Flows With Vortex Filaments", Lecture Notes in Physics 59, Proc. 5th International Conference on Numerical Methods in Fluid Dynamics, 280, Springer-Verlag, Berlin (1976).
3. J.C.S. Meng, "The Physics of Vortex-Ring Evolution in a Stratified and Shearing Environment", Journal of Fluid Mechanics 84, 455 (1978).
4. A. J. Chorin, "Numerical Study of Slightly Viscous Flow", Journal of Fluid Mechanics 57, 785 (1973).
5. J. P. Christiansen, "Numerical Simulation of Hydrodynamics by the Method of Point Vortices", Journal Comp. Physics 13, 363-379 (1973).
6. R. S. Rogallo, "Proc. AIAA 2nd Comp. Fluid Dyn. Conf.", AIAA, 67 (1975).
7. W. T. Ashurst, "Numerical Simulation of Turbulent Mixing Layer Via Vortex Dynamics", Proc. 1st Intl. Symp. on Turbulent Shear Flows, Penn. State University (1977).
8. J.C.S. Meng and J.A.L. Thomson, "Numerical Studies of Some Non-linear Hydrodynamic Problems by Discrete Vortex Element Methods", Journal of Fluid Mechanics 84, 433 (1978).

9. J. P. Christiansen and K. V. Roberts, Papers 40 and 52, Proc. of Comp. Physics Conference, Culham Laboratory (1969).

10. B. Alder, S. Fernbach, N. Rotenberg, Eds., "Method of Computational Physics" 9, Academic Press, New York (1970).

11. S. S. Wang, "Grid-Insensitive Computer Simulation of the Kelvin-Helmholtz Instability and Shear Flow Turbulence", Ph.D. thesis SU-IPR Report No. 710, Stanford University (1977).

12. O. Buneman, "The Advance From 2-D Electrostatic to 3-D Electromagnetic Particle Simulation", Computer Physics Comm 12, 21-31 (1976).

13. S. A. Orszag, "Lectures on the Statistical Theory of Turbulence", Flow Research Report #31 (1974).

14. S. A. Orszag and G. S. Patterson, "Numerical Simulation of Three-Dimensional Homogeneous Isotropic Turbulence", Phys. Rev. Lett. 28, 76-79 (1972). Also "Statistical Models and Turbulence", Springer-Verlag, 127-147.

15. S. A. Orszag and D. S. Raila, "Test of Spectral Energy Transfer Models of Turbulence Decay", Phys. Fluids 16, 172-173 (1973).

16. D. G. Fox and S. A. Orszag, "Inviscid Dynamics of Two-Dimensional Turbulence", Phys. Fluids 16, 169-171 (1973).

17. S. A. Orszag, "Numerical Simulation of Incompressible Flows Within Simple Boundaries. I. Galerkin (Spectral) Representations", Studies in Appl. Math. 50, 293-327 (1971).

18. M. Abramowitz and S. A. Stegun, Handbook of Mathematical Functions, National Bureau of Standards (1968).

19. O. Buneman, "Variationally Optimized, Grid-Insensitive Vortex Tracing", Lecture Notes in Physics 35, Proc. 4th International Conference on Numerical Methods in Fluid Dynamics, Springer-Verlag, Berlin (1975).

20. R. W. Hamming, Numerical Methods for Scientists and Engineers, 2nd ed., McGraw-Hill (1973).

21. P. G. Saffman, "The Velocity of Viscous Vortex Rings", Studies in Applied Mathematics, Vol. XLIX, No. 4, December 1970.

22. G. I. Taylor and A. E. Green, "Mechanism of the Production of Small Eddies from Large Ones", Proc. Roy. Soc. A158, 499-521 (1937).

23. S. Goldstein, "Three-Dimensional Vortex Motion in a Viscous Fluid", Phil. Magazine 30, 85-102 (1940).

24. S. A. Orszag, "Numerical Simulation of the Taylor-Green Vortex", Computing Methods in Applied Science and Engineering, ed. R. Glowinski and J. L. Lions, Springer (1974).

25. R. Betchov and A. A. Szewczyk, "Numerical Study of the Taylor-Green Vortices", Phys. Fluids 21, 871 (1978).

26. E. L. Lindman, "'Free-Space' Boundary Conditions for the Time Dependent Wave Equation", Journal of Comp. Physics 18, 66 (1975).

27. R. A. James, "The Solution of Poisson's Equation for Isolated Source Distributions", Journal of Comp. Physics 25, 71-93 (1977).